Cellular/Molecular

# An AnkyrinG-Binding Motif Is Necessary and Sufficient for Targeting $Na_v1.6$ Sodium Channels to Axon Initial Segments and Nodes of Ranvier

**Andreas Gasser,[1,2,3]* Tammy Szu-Yu Ho,[4]* Xiaoyang Cheng,[1,2,3] Kae-Jiun Chang,[4] Stephen G. Waxman,[1,2,3] Matthew N. Rasband,[4,5] and Sulayman D. Dib-Hajj[1,2,3]**

[1]Department of Neurology and [2]Center for Neuroscience and Regeneration Research, Yale University School of Medicine, New Haven, Connecticut 06510, [3]Rehabilitation Research Center, Veterans Administration Connecticut Healthcare System, West Haven, Connecticut 06516, and [4]Program in Developmental Biology and [5]Department of Neuroscience, Baylor College of Medicine, Houston, Texas 77030

**Neurons are highly polarized cells with functionally distinct axonal and somatodendritic compartments. Voltage-gated sodium channels $Na_v1.2$ and $Na_v1.6$ are highly enriched at axon initial segments (AISs) and nodes of Ranvier, where they are necessary for generation and propagation of action potentials. Previous studies using reporter proteins in unmyelinated cultured neurons suggest that an ankyrinG-binding motif within intracellular loop 2 (L2) of sodium channels is sufficient for targeting these channels to the AIS, but mechanisms of channel targeting to nodes remain poorly understood. Using a CD4-$Na_v1.2$/L2 reporter protein in rat dorsal root ganglion neuron–Schwann cell myelinating cocultures, we show that the ankyrinG-binding motif is sufficient for protein targeting to nodes of Ranvier. However, reporter proteins cannot capture the complexity of full-length channels. To determine how native, full-length sodium channels are clustered in axons, and to show the feasibility of studying these channels *in vivo*, we constructed fluorescently tagged and functional mouse $Na_v1.6$ channels for *in vivo* analysis using *in utero* brain electroporation. We show here that wild-type tagged-$Na_v1.6$ channels are efficiently clustered at nodes and AISs *in vivo*. Furthermore, we show that mutation of a single invariant glutamic acid residue (E1100) within the ankyrinG-binding motif blocked $Na_v1.6$ targeting in neurons both *in vitro* and *in vivo*. Additionally, we show that caseine kinase phosphorylation sites within this motif, while not essential for targeting, can modulate clustering at the AIS. Thus, the ankyrinG-binding motif is both necessary and sufficient for the clustering of sodium channels at nodes of Ranvier and the AIS.**

## Introduction

Integration of signals at action potential trigger zones and high-fidelity signal transmission along axons require high densities of voltage-gated sodium channels (VGSCs) at axon initial segments (AISs) and nodes of Ranvier (Hille, 2001). Neuronal excitability can be regulated by activity-dependent relocation (Grubb and Burrone, 2010) or resizing (Kuba et al., 2010) of the AIS, and the density and properties of VGSCs at the AIS, and their distance from the soma determine the threshold for action potential firing (Fried et al., 2009). The VGSC $Na_v1.6$ is enriched at the AIS in most CNS neurons (Vacher et al., 2008), replaces $Na_v1.2$ during maturation of nodes in CNS neurons (Boiko et al., 2001; Kaplan et al., 2001), and is the main channel at both immature and mature nodes in the PNS (Schafer et al., 2006). Mice that lack $Na_v1.6$ (Burgess et al., 1995), at sites that include nodes of Ranvier (Black et al., 2002), are juvenile lethal, suggesting that $Na_v1.6$ is essential for nerve conduction after compact myelin formation.

VGSC accumulation at the AIS and nodes of Ranvier is thought to depend on ankyrinG (ankG), which anchors channels to a spectrin-dependent cytoskeletal network (Bennett and Lambert, 1999; Jenkins and Bennett, 2001; Dzhashiashvili et al., 2007). A highly conserved 9 aa motif in intracellular loop 2 (L2) of VGSCs is required for binding ankG (Lemaillet et al., 2003). The role of this motif in VGSC localization thus far has been inferred from studies using chimeric reporter proteins constructed from Neurofascin 186 (Lemaillet et al., 2003), CD4 (Garrido et al., 2003), or $K_v2.1$ (Garrido et al., 2003) fused to $Na_v1.2$/L2. These studies show that the ankG-binding motif is sufficient for AIS targeting in cultured hippocampal neurons (Garrido et al., 2003; Lemaillet et al., 2003). Although these chimera studies have proven to be very informative, they have several important limitations: first, the experiments do not test whether the motif and its interactions with ankG are necessary for AIS clustering of full-length channels and cannot exclude the

Received Oct. 27, 2011; revised March 15, 2012; accepted March 25, 2012.

Author contributions: A.G., S.G.W., M.N.R., and S.D.D.-H. designed research; A.G., T.S.-Y.H., X.C., and K.-J.C. performed research; A.G., T.S.-Y.H., X.C., K.-J.C., M.N.R., and S.D.D.-H. analyzed data; A.G., S.G.W., M.N.R., and S.D.D.-H. wrote the paper.

This work was supported by grants from the Rehabilitation Research Service and Medical Research Service, Department of Veterans Affairs (S.D.D.-H., S.G.W.), and by NIH Grants R01NS044916 and R01NS069688 (M.N.R.). We acknowledge Dr. Joel Black for helpful discussions, Dr. Peng Zhao for transfecting hippocampal neurons for electrophysiology experiments, and the technical assistance of Lynda Tyrrell and Palak Shah. The Center for Neuroscience and Regeneration is a Collaboration of the Paralyzed Veterans of America with Yale University.

*A.G. and T.S.-Y.H. contributed equally to this work.

Correspondence should be addressed to Dr. Sulayman D. Dib-Hajj, The Center for Neuroscience and Regeneration Research, 127A, Building 34, Veterans Affairs Connecticut Healthcare System, 950 Campbell Avenue, West Haven, CT 06516. E-mail: sulayman.dib-hajj@yale.edu.

A. Gasser's present address: Department of Trauma, Hand, and Reconstructive Surgery, University Medical Center Hamburg-Eppendorf, Hamburg, Germany.

DOI:10.1523/JNEUROSCI.5434-11.2012

 0270-6474/12/327232-12$15.00/0

possibility that other interactions, unrelated to ankG binding, are also sufficient for VGSC localization. Second, studies using $K_v2.1$ as a reporter protein are complicated by the fact that these channels exist as homotetramers and AIS accumulation might occur with chimeras due to high avidity even when affinity is reduced. Third, a recent report demonstrated that $K_v2.1$ accumulates at the AIS of hippocampal neurons in culture (Sarmiere et al., 2008). Fourth, the experiments performed to date have all been done in unmyelinated, cultured neurons, precluding discovery of the mechanism of VGSC channel clustering at nodes of Ranvier. Thus, these studies cannot capture the full complexity of native channels and their clustering in axons *in vivo*.

To overcome these limitations, we have used full-length functional $Na_v1.6$ channels to analyze the role of the ankG-binding motif in VGSC channel targeting at the AIS and nodes of Ranvier. We present here evidence that the ankG-binding motif is both necessary and sufficient for the clustering of VGSCs at AISs and nodes of Ranvier.

## Materials and Methods

*Antibodies.* Chicken polyclonal anti-MAP2 antibody was obtained from Encor Biotechnology, and mouse monoclonal anti-ankyrin G antibody (clone N106/36) and Caspr antibody (clone K65/35) were from University of California at Davis/NIH NeuroMab Facility (Davis, CA). Rabbit anti-GFP was purchased from Invitrogen. Rat monoclonal anti-MBP was from Millipore (MAB386), and rat monoclonal anti-RFP (to detect mCherry) was purchased from Allele Biotechnology. Secondary antibodies for immunolabeling were Cy5 donkey anti-chicken, DyLight 549 donkey anti-mouse, DyLight 649 donkey anti-mouse, Dylight 594 goat anti-rat, AMCA goat anti-mouse IgG (Jackson ImmunoResearch), and Alexa Fluor 488 goat anti-rabbit (Invitrogen).

*DNA constructs.* The CD4-L2-EGFP was constructed by inserting the $Na_v1.2$/L2 sequence from pCB6-CD4-$Na_v1.2$ II-III into the AgeI site between CD4 and EGFP in pCX-CD4-EGFP, which contains the extracellular domain, transmembrane domain, and first three cytosolic amino acid residues of human CD4 fused to EGFP (pCB6-CD4-$Na_v1.2$ II-III; kindly provided by Dr. Benedict Dargent, Université de la Méditerranée, Marseille, France; CD4-EGFP fusion was constructed by Dr. Yasuhiro Ogawa, Meiji Phamaceutical University, Japan). The CD4-L2(ΔABD)-EGFP was constructed by deleting the 9 aa residues VPIALGESD (corresponding to residues 1094–1102 in mouse $Na_v1.6$) from the CD4-L2-EGFP.

To obtain a construct encoding full-length $Na_v1.6$ fused to EGFP, the plasmid pcDNA3-$Na_v1.6_R$, which encodes full-length mouse $Na_v1.6$ rendered resistant to tetrodotoxin (TTX-R) by the substitution Y371S (Herzog et al., 2003) was modified as follows: (1) we introduced a unique KpnI restriction site into the parental plasmid replacing the translation termination codon (TAG), and generated a unique XbaI restriction site 3′ of the KpnI site, using the QuikChange II XL mutagenesis kit (Stratagene); (2) the coding sequence for EGFP was then cut out from pEGFP-N3 (BD Biosciences) with the same enzymes, and cloned into the KpnI and XbaI sites of modified pcDNA3-$Na_v1.6_R$, resulting in the fusion of EGFP to the C terminus of the $Na_v1.6$ open reading frame with a spacer sequence of 10 aa (GTAGPGSIAT); (3) we increased the length of this linker to 19 aa (GTRILQSTVGTAGPGSIAT) by insertion of oligonucleotides into the KpnI site, which improved the intensity of green fluorescence of the fusion protein, and generated a unique ApaI site. This final plasmid construct will be referred to a as pcDNA3-$Na_v1.6$-EGFP hereinafter. The mutations V1098P and E1100A were introduced into pcDNA3-$Na_v1.6$-EGFP with the QuikChange II XL mutagenesis kit. To generate a C-terminal fusion of the red fluorescence protein mCherry to $Na_v1.6$, the plasmid pcDNA3-$Na_v1.6$-EGFP was digested with ApaI and XbaI to remove the EGFP sequence. The open reading frame of mCherry was then amplified from the plasmid pLVX-IRES-mCherry (Promega) with primers introducing the appropriate restriction sites, and subcloned into the ApaI/XbaI-digested backbone of pcDNA3-$Na_v1.6$-EGFP to yield the construct pcDNA3-$Na_v1.6$-mCherry.

| | | | |
|---|---|---|---|
| $Na_v1.1$ | 1108 | NPSLTVTVPIAVGESDFENLNTEDFSSESDLEE | Mum |
| | 1108 | NPSLTVTVPIAVGESDFENLNTEDFSSESDLEE | Rnor |
| | 1098 | NPSLTVTVPIAVGESDFENLNTEDFSSESDLEE | Hs |
| $Na_v1.2$ | 1097 | NPSLTVTVPIAVGESDFENLNTEDFSSESDLEE | Mum |
| | 1098 | NPSLTVTVPIALGESDFENLNTEEFSSESDMEE | Rnor |
| | 1098 | NPSLTVTVPIAVGESDFENLNTEEFSSESDMEE | Hs |
| $Na_v1.3$ | 1046 | NPSLTVTVPIAVGESDFENLNTEEFSSESELEE | Mum |
| | 1047 | NPSLTVTVPIAVGESDFENLNTEEFSSESELEE | Rnor |
| | 1096 | NPSLTVTVPIAVGESDFENLNTEEFSSESELEE | Hs |
| $Na_v1.4$ | 911 | NPYLTIHVPIASEESDLEMPTEEETDTFSEPED | Mum |
| | 910 | NPYLTIQVPIASEESDLEMPTEEETDAFSEPED | Rnor |
| | 917 | NPYLTIQVPIASEESDLEMPTEEETDTFSEPED | Hs |
| $Na_v1.5$ | 1047 | -----VCVPIAVAESDTDDQEEDEENS-LGTEE | Mum |
| | 1048 | -----VCVPIAVAESDTEDQEEDEENS-LGTEE | Rnor |
| | 1045 | -----VCVPIAVAESDTDDQEEDEENS-LGTEE | Hs |
| $Na_v1.6$ | 1078 | NPSLTVTVPIAVGESDFENVNTEEFSSESELEE | Oa |
| | 1065 | NPNLTVCVPIAVGESDFENLNTEDFSSESDIEN | Tr |
| | 1061 | NPNLTVCVPIAVGESDFENLNTEDFSSESDIEN | Tn |
| | 1058 | NPNLTVCVPIAVGESDFENLNTEDFSSESEAEG | Dr |
| | 1088 | NPNLTVKVPIAVGESDFENLNTEDFSSASDEEG | Xt |
| | 1089 | NPNLTVRVPIAVGESDFENLNTEDFSSDTDPDG | Ac |
| | 1089 | NPNLTVRVPIAVGESDFENLNTEDVSSESDPEG | Gg |
| | 1112 | NPSLTVTVPIAVGESDFENLNTEEFSSESDLEE | Md |
| | 1087 | NPNLTVRVPIAVGESDFENLNTEDVSSESDPEG | Mum |
| | 1097 | NPNLTVRVPIAVGESDFENLNTEDVSSESDPEG | Rnor |
| | 1086 | NPNLTVRVPIAVGESDFENLNTEDVSSESDPEG | Am |
| | 1089 | NPNLTVRVPIAVGESDFENLNTEDVSSESDPEG | Oc |
| | 1092 | NPNLTVRVPIAVGESDFENLNTEDVSSESDPEG | Cf |
| | 1090 | NPNLTVRVPIAVGESDFENLNTEDVSSESDPEG | Ec |
| | 1089 | NPNLTVRVPIAVGESDFENLNTEDVSSESDPEG | Bt |
| | 1088 | NPNLTVRVPIAVGESDFENLNTEDVSSESDPEG | Cj |
| | 1089 | NPNLTVRVPIAVGESDFENLNTEDVSSESDPEG | Hl |
| | 1089 | NPNLTVRVPIAVGESDFENLNTEDVSSESDPEG | Mmu |
| | 1089 | NPNLTVRVPIAVGESDFENLNTEDVSSESDPEG | Pt |
| | 1089 | NPNLTVRVPIAVGESDFENLNTEDVSSESDPEG | Hs |
| $Na_v1.7$ | 1078 | NPSLTVTVPIALVESDFENVNTEEFSSESDVDG | Oa |
| | 1072 | NPSLTVTVPIAQGESDFENVNTEEFSSESDVEG | Md |
| | 1070 | NPSLTVTVPIAPGESDLENMNTEELSSDSDSDY | Mum |
| | 1081 | NPSLTVTVPIAPGESDLEIMNTEELSSDSDSDY | Rnor |
| | 1079 | NPSLTVTVPIAPGESDLENMNTEELSSDSESEY | Oc |
| | 1081 | NPSLTVTVPIAPGESDLENMNTEELSSDSDSEY | Cf |
| | 1069 | NPSLTVTVPIAPGESDLENMNTEELSSDSESEY | Ec |
| | 1070 | NPSLTVTVPIAPGESDLEIMNTEELSSDSDSEY | Bt |
| | 1069 | NPSLTVTVPIAPGESDLENMNTEELSSDSDSEY | Mam |
| | 1071 | NPSLTVTVPIAPGESDLENMNAEELSSDSDSEY | Hs |
| $Na_v1.8$ | 991 | DPNVWVSVPIAEGESDLDELEEDVEQASQSSWQ | Mum |
| | 991 | DPNVWVSVPIAEGESDLDELEEDMEQASQSSWQ | Rnor |
| | 992 | NPTVWVSVPIAEGESDLDDLEDDGGEDAQSFQQ | Hs |
| $Na_v1.9$ | 895 | -------APLAK---EEDDMECCGECDASPTSQ | Mum |
| | 894 | -------APLAE---VEDDVEYCGEGGALPTSQ | Rnor |
| | 917 | -------APLAE---EEDDVEFSGEDNAQRITQ | Hs |

**Figure 1.** Phylogenetic conservation of the ankyrinG-binding motif in voltage-gated sodium channels from vertebrates. $Na_v1.1$: *Mus musculus* (Mum) (mouse), A2APX8_MOUSE; *Rattus norvegicus* (Rnor) (rat), NP_110502; *Homo sapiens* (Hs) (human), NP_001159435. $Na_v1.2$: Mum, A2APX6_MOUSE; Rnor, NP_036779; Hs, NP_001035232. $Na_v1.3$: Mum, NP_001092768; Rnor, NP_036779; Hs, NP_001075145. $Na_v1.4$: Mum, NP_573462; Rnor, NP_037310; Hs, NP_000325. $Na_v1.5$: Mum, NP_067519; Rnor, NP_001153634; Hs, NP_932173. $Na_v1.6$: *Ornithorhynchus anatinus* (Oa) (duckbill platypus), F6VX76_ORNAN; *Takifugu rubripes* (Tr) (Japanese pufferfish), UPI00016E65FF; *Tetraodon nigroviridis* (Tn) (pufferfish), Q4RVW9_TETNG; *Danio rerio* (Dr) (zebrafish), AF297658; *Xenopus tropicalis* (Xt) (frog), F6XFJ2_XENTR; *Anolis carolinensis* (Ac) (chameleon), XP_003216968; *Gallus gallus* (Gg) (chicken), Q9UQD0; *Monodelphis domestica* (Md) (gray short-tail oppossum), F7EYW6_MONDO; Mum, NP_035453; Rnor, NP_062139; *Ailuropoda melanoleuca* (Am) (panda), XP_002921605; *Oryctolagus cuniculus* (Oc) (rabbit), XP_002711236; *Canis familiaris* (Cf) (dog), XP_850134; *Equus caballus* (Ec) (horse), F7AP65_Horse; *Bos taurus* (Bt) (bovine), NP_001180031; *Callithrix jacchus* (Cj) (common marmoset), F7GQB4_CALJA; *Hylobates leucogenys* (Hl) (white-cheeked gibbon), XP_003252169; *Macaca mulatta* (Mmu) (rhesus macaque), F7ADS8_MACMU; *Pan troglodytes* (Pt) (common chimpanzee), XP_001141985; Hs, NP_055006. $Na_v1.7$: Md, XP_001367438; Mum, Q62205; Rnor, NP_579823; Oc, Q28644; Cf, XP_859026; Ec, XP_001496473; Bt, XP_001252616; Mmu, XP_001101662; Hs, Q15858. $Na_v1.8$: Mum, NP_033160; Rnor, NP_058943; Hs, NP_006505; $Na_v1.9$: Mum, NP_036017; Rnor, NP_062138; Hs, NP_054858.

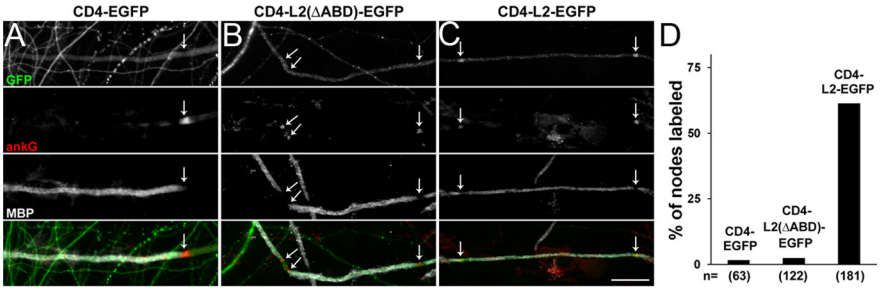


**Figure 2.** The ankG-binding motif is sufficient for protein clustering at nodes of Ranvier. ***A–C***, DRG neurons transfected with plasmids encoding CD4-EGFP (***A***), CD4-L2(ΔABD)-EGFP (***B***), and CD4-L2-EGFP (***C***) chimeric proteins were cocultured with myelinating Schwann cells. Nodes of Ranvier and heminodes (indicated by arrows) were delineated by ankG immunostaining (red), and the myelin sheaths were detected with MBP antibodies (white). Chimeric proteins were detected with GFP antibodies (green). Scale bar, 20 μm. ***D***, The numbers of nodes and heminodes with enriched chimeric protein localization were expressed as the percentage of ankG labeled nodes.

For expression of the $Na_v1.6$ fusion proteins *in vivo*, the CMV promoter in the pcDNA3-derived vectors was replaced by the human elongation factor-1 α (EF-1 α) promoter. To this end, the CMV promoter was excised from pcDNA3 constructs using NruI and NheI restriction enzymes. The restriction sites were blunted with T4 polymerase and religated, which restored the NheI restriction site. The EF-1 α promoter was then amplified from pEF α vector introducing NheI restriction sites on both ends, and subcloned into the NheI site of the promotorless plasmid carrying the $Na_v1.6$ fusion protein. A similar procedure was used to generate the plasmids pcEF-$Na_v1.6$-EGFP and pcEF-$Na_v1.6$-mCherry for *in utero* electroporation experiments. The mutations V1098P (VP), E1100A (EA), S1112–1113A (SSAA), S1115A (SA), and S1101A/S1112–1113A/S1115A (4SA) were introduced into pcEF-$Na_v1.6$-EGFP by site-directed mutagenesis using the QuikChange II XL kit. All clones were verified by sequence analysis and their functionality was tested by transient expression in the neuronal ND7/23 cell line. Twenty-four hours after transfection, the cells were analyzed for fluorescence and production of TTX-R currents.

*Myelinating coculture.* All work involving animals complied with NIH guidelines and has been approved by the Institutional Animal Care and Use Committee at the Veterans Administration Connecticut Healthcare System or Baylor College of Medicine. Myelinating coculture was performed as described previously (Susuki et al., 2011). Briefly, dorsal root ganglia (DRGs) were dissected from embryonic day 18 Sprague Dawley rats of either sex (Harlan Laboratories), dissociated, and plated on glass coverslips coated with Matrigel (BD Biosciences). DRG neurons were purified by two cycles of antimitotic treatment and then transfected with the CD4-EGFP, CD4-L2-EGFP, or CD4-L2(ΔABD)-EGFP plasmids using Lipofectamine LTX and PLUS reagents (Invitrogen) after 9 d *in vitro* (DIV). Purified rat Schwann cells were added at 10 DIV. Myelination was induced at 15 DIV by the addition of 50 μg/ml ascorbic acid. Cells were fixed in 4% paraformaldehyde at 4°C for 20 min at 32 DIV (17 d after the induction of myelination), followed by immunostaining as described previously (Hedstrom et al., 2007). Both heminodes and nodes were analyzed.

*Hippocampal neuron isolation and transfection.* Sprague Dawley rat pups of either sex between postnatal day 0 (P0) and P2 were anesthetized with ketamine/xylazine (100/10 mg/kg, i.p.) and killed by decapitation. Hippocampal neurons were isolated and transfected as previously described (Estacion et al., 2010). Hippocampi were quickly dissected out in ice-cold HABG [HA medium (Brain Bits) supplemented with 2% B-27 and 0.5 mM Glutamax (Invitrogen)], sliced into 350 μm sections using a McIlwain tissue chopper (Warner Instruments), and digested (30 min at 30°C) with papain (30 U/ml; Worthington) in calcium-free HA medium (Brain Bits) with 0.5 mM Glutamax. After digestion, tissue was resuspended in HABG and triturated with two fire-polished glass pipettes of decreasing apertures. After settling of bulk tissue, the supernatant was filtered through a 40 μm mesh and centrifuged at 1000 × *g* (4 min, room temperature). For transfection, hippocampal neurons were resuspended in 200 μl of buffer R (Neon kit; Invitrogen) at a density of ~0.5 × $10^7$cells/ml. Ten microliter aliquots were transfected by electroporation (MicroPorator; Harvard Apparatus; two pulses, each 15 ms, of 1500 V) using 0.5 μg of plasmid DNA per transfection. For transfection of wild-type $Na_v1.6$-EGFP or $Na_v1.6$-mCherry as well as the $Na_v1.6$-VP-EGFP and $Na_v1.6$-EA-EGFP mutants, we used plasmids with CMV or EF-1 α promoters without any notable difference. For the channel mutants $Na_v1.6$-SSAA-EGFP, $Na_v1.6$-SA-EGFP, and $Na_v1.6$–4SA-EGFP, we only used expression constructs driven by the EF-1 α promoter. In cases of double transfections with two channel constructs expressing EGFP and mCherry, cells were transfected with 0.5 μg of each plasmid. Following electroporation, cells were resuspended in 45 μl of calcium-free HABG medium and incubated for 5 min at room temperature. Forty-five microliters of complete medium [Neurobasal medium, supplemented with 2% B-27, 0.5 mM Glutamax, and 10 μg/ml gentamycin (Invitrogen)] was added. Cells were plated on 12 mm glass coverslips coated with poly-D-lysine and laminin (BD Biosciences,), placed in a 24-well plate, and incubated at 37°C for 1 h to allow attachment. Finally, 500 μl/well complete medium was added, and cells were incubated at 37°C until use. One-half of the medium was exchanged after 3 d, and cells were used for immunocytochemistry after 6 d in culture.

In utero *electroporation. In utero* electroporation of WT and mutant $Na_v1.6$ plasmids was performed in E14 mouse embryos of either sex as described previously (Hedstrom et al., 2007). Mice were subsequently killed at P5 or P27, followed by sectioning and immunostaining as described previously (Hedstrom et al., 2007).

*Immunocytochemistry.* Cells were washed once with PBS and fixed for 10 min with 4% paraformaldehyde in 0.14 M Sorensen's phosphate buffer. After another wash with PBS, cells were sequentially incubated in the following solutions: (1) blocking solution (PBS/3% cold water fish gelatin/3% newborn donkey serum/0.1% Triton X-100) for 30 min at room temperature, (2) primary antibodies in blocking solution at 4°C overnight, (3) six PBS washes for 5 min each, (4) secondary antibodies in blocking solution at 4°C overnight, (5) six PBS washes for 5 min each. Coverslips were then mounted with Aqua-Poly/Mount (Polysciences), and images were acquired with a Nikon E600 microscope equipped with confocal optics. For *in vivo* data, *z*-stack images of brain sections were taken using a Zeiss Axioimager Z1 microscope fitted with an Apotome for optical sectioning of the tissue.

*Image analysis.* To obtain a quantitative measure of $Na_v1.6$ localization at the AISs, fluorescence images were analyzed with NIH ImageJ software. The ankG and the MAP2 signals, respectively, were used to define two regions of interests using the ImageJ tracing tool, which represent either the AISs (ankG) or the somatodendritic (MAP2) neuronal compartments. For each cell, average EGFP intensities were then quantified for both regions, and the EGFP intensity at the AISs was normalized to the EGFP intensity in the somatodendritic compartment. Brightness and contrast of the acquired fluorescence images were uniformly enhanced using ImageJ for the purpose of presentation.

*Voltage-clamp electrophysiology.* Whole-cell voltage-clamp recordings were performed with an Axopatch 200B amplifier (Molecular Devices) at room temperature. Fire-polished electrodes were fabricated from 1.6 mm outer-diameter borosilicate glass micropipettes (World Precision Instruments). Pipette potential was adjusted to zero before seal formation, and liquid junction potential was not corrected. Capacity transients were cancelled and series resistance was compensated by 70–90%. Leakage current was subtracted digitally on-line using hyperpolarizing potentials applied after the test pulse (P/6 procedure). Currents were acquired with Clampex 9.2, 5 min after establishing whole-cell configuration, sampled at a rate of 100 or 50 kHz, and filtered at 5 kHz.

ND7/23 cells were transfected with untagged $Na_v1.6_R$ plus GFP (4:1), $Na_v1.6$-EGFP, $Na_v1.6$-mCherry, or $Na_v1.6$-EGFP mutant (EA, SA, SSAA, 4SA) derivatives using Lipofectamine 2000 (Invitrogen) as previously described (Wittmack et al., 2004, 2005; Rush et al., 2006), and sodium currents were recorded at 20–36 h after transfection. Cells were held at

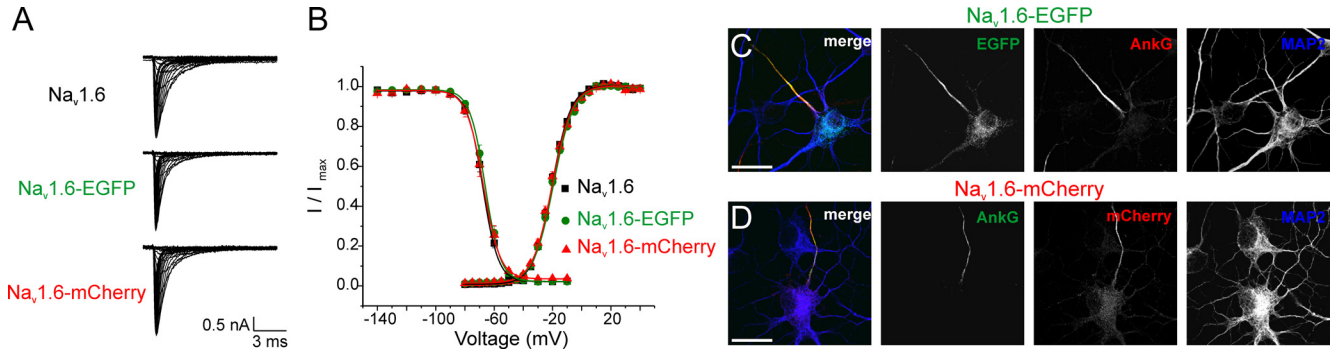


**Figure 3.** Fusion of EGFP or mCherry to the C terminus of $Na_v1.6$ does not alter channel gating properties or clustering at the AIS. ***A***, Representative families of sodium currents in DRG-derived cell line ND7/23 transfected with $Na_v1.6$, $Na_v1.6$-EGFP, or $Na_v1.6$-mCherry show comparable amplitudes and kinetics of activation and fast inactivation. ***B***, Boltzmann fits for voltage dependence of activation and steady-state fast inactivation of $Na_v1.6$-EGFP and $Na_v1.6$-mCherry are similar to those of untagged $Na_v1.6$ channels. Data are presented as mean values ± SEM ($n = 7$–22, as detailed in Table 1). ***C***, ***D***, Fluorescent tags at $Na_v1.6$ C terminus do not impair channel targeting to the AIS in hippocampal neurons. P0–P2 rat hippocampal neurons were transfected with $Na_v1.6$, $Na_v1.6$-EGFP (***C***), or $Na_v1.6$-mCherry (***D***). After 6 d in culture, cells were fixed and stained for MAP2 and ankG, and fluorescence was analyzed by confocal microscopy. Green fluorescence of $Na_v1.6$-EGFP (***C***) as well as red fluorescence of $Na_v1.6$-mCherry (***D***) were detectable at the AIS, which were identified by ankG staining (yellow). Fluorescently tagged $Na_v1.6$ channels were not present in MAP2-positive dendrites. Scale bars, 20 $\mu$m.

**Table 1. Current density and gating properties of wild-type and mutant $Na_v1.6_R$ channels**

| Channel | Current density (pA/pF)[b] | Reversal potential (mV) | Activation | | | Steady-state fast inactivation | | |
|---|---|---|---|---|---|---|---|---|
| | | | $V_{1/2,act}$ | $k$ | $n$ | $V_{1/2,fast}$ | $k$ | $n$ |
| **$Na_v1.6$ + EGFP** | 88.4 ± 8.7 (28) | 69.9 ± 0.7 | −21.0 ± 0.5 | −6.55 ± 0.13 | 16 | −67.9 ± 0.9 | 5.41 ± 0.12 | 15 |
| **$Na_v1.6$-EGFP** | 79.5 ± 10.0 (26) | 69.6 ± 0.8 | −20.2 ± 0.5 | −7.09 ± 0.17 | 19 | −66.3 ± 1.0 | 5.50 ± 0.10 | 8 |
| $Na_v1.6$-mCherry | 79.2 ± 10.7 (33) | 68.4 ± 1.0 | −21.0 ± 0.7 | −6.96 ± 0.23 | 22 | −67.6 ± 1.6 | 5.88 ± 0.36 | 7 |
| **$Na_v1.6$-EGFP** | 77.4 ± 9.8 (34) | 73.8 ± 0.7 | −19.2 ± 0.4 | −7.27 ± 0.16 | 21 | −65.3 ± 0.8 | 5.71 ± 0.13 | 20 |
| $Na_v1.6$-VP-EGFP | 80.9 ± 12.3 (32) | 73.2 ± 1.2 | −18.9 ± 1.0 | −7.28 ± 0.2 | 16 | −65.8 ± 1.2 | 6.12 ± 0.24 | 15 |
| $Na_v1.6$-EA-EGFP | 72.5 ± 12.4 (29) | 74.1 ± 1.2 | −17.8 ± 0.9 | −7.44 ± 0.33 | 11 | −68.4 ± 1.1 | 6.09 ± 0.20 | 11 |
| **$Na_v1.6$-EGFP**[a] | 72.1 ± 10.3 (23) | 69.7 ± 0.9 | −20.1 ± 0.6 | −7.18 ± 0.17 | 17 | −66.0 ± 1.2 | 6.29 ± 0.27 | 10 |
| $Na_v1.6$-mCherry[a] | 84.9 ± 12.9 (26) | 67.9 ± 1.0 | −21.3 ± 0.8 | −7.03 ± 0.26 | 18 | −66.9 ± 0.6 | 6.45 ± 0.41 | 10 |
| $Na_v1.6$-SSAA-EGFP[a] | 75.1 ± 6.3 (22) | 69.8 ± 0.8 | −20.0 ± 0.4 | −6.95 ± 0.14 | 20 | −65.8 ± 0.7 | 5.63 ± 0.12 | 13 |
| $Na_v1.6$-SA-EGFP[a] | 86.5 ± 9.6 (22) | 70.6 ± 0.7 | −19.9 ± 0.6 | −7.06 ± 0.21 | 15 | −66.2 ± 0.7 | 6.00 ± 0.27 | 12 |
| **$Na_v1.6$-EGFP**[a] | 118.3 ± 13.7 (15) | 72.8 ± 1.3 | −20.4 ± 0.7 | −6.10 ± 0.23 | 13 | −61.9 ± 1.0 | 5.45 ± 0.10 | 13 |
| $Na_v1.6$–4SA[a] | 123.5 ± 20.2 (18) | 71.4 ± 1.1 | −18.9 ± 0.6 | −6.33 ± 0.22 | 16 | −61.4 ± 0.9 | 5.47 ± 0.14 | 12 |

Data were obtained from four independent sets of experiments. Statistical significance for each set was determined by comparison to the corresponding wild-type control channel (bold face type). Data are shown as mean values ± SEM.

[a]The length of prepulses of steady-state fast inactivation was 100 ms, instead of 500 ms.

[b]The number of ND7/23 cells recorded is shown in parentheses.

−120 mV after break-in. For current–voltage relationships, cells were held at −120 mV and stepped to a range of potentials (−80 to +60 mV in 5 mV increments) for 100 ms each. Peak inward currents ($I$) were plotted as a function of depolarizing potential to generate $I$–$V$ curves. Activation curves were obtained by converting $I$ to conductance ($G$) at each voltage ($V$) using the equation: $G = I/(V - V_{rev})$, where $V_{rev}$ is the reversal potential that was determined for each cell individually. Activation curves were fit with Boltzmann function in the form of $G = G_{max}/\{1 + \exp[(V_{1/2,act} - V)/k]\}$, where $G_{max}$ is the maximal sodium conductance, $V_{1/2,act}$ is the potential at which activation is half-maximal, $V$ is the test potential, and $k$ is the slope factor. Steady-state fast inactivation was achieved with a series of 100 or 500 ms prepulses (−140 to −10 mV in 10 mV increments), and the non-inactivated channels were measured by a 40 ms test pulse to −10 mV. Peak inward currents obtained from steady-state fast inactivation were normalized to the maximal peak current ($I_{max}$) and fit with Boltzmann function in the form of $I/I_{max} = A + (1 - A)/\{1 + \exp[(V - V_{1/2,inact})/k]\}$, where $V$ represents the inactivating prepulse potential, $V_{1/2,inact}$ represents the midpoint of inactivation curve, and $A$ is the offset.

The pipette solution contained the following (in mM): 140 CsF, 10 NaCl, 1 EGTA, and 10 HEPES, pH 7.30 (with CsOH), and osmolarity was adjusted to 316 mOsmol/L with dextrose. The extracellular solution contained the following (in mM): 140 NaCl, 3 KCl, 20 TEA·Cl (tetraethylammonium chloride), 1 $MgCl_2$, 1 $CaCl_2$, 10 HEPES, 5 CsCl, 0.1 $CdCl_2$, pH 7.32 (with NaOH), and the osmolarity was 330 mOsmol/L. Tetrodotoxin (300 nM) was added to the extracellular bath solution to block endogenous voltage-gated sodium currents (Wittmack et al., 2004, 2005; Rush et al., 2006).

To assess the effect of E1100A on $Na_v1.6$ current in native neurons, WT $Na_v1.6_R$-EGFP or $Na_v1.6_R$-EA-EGFP were transfected into P0–P5 rat (either sex) hippocampal neurons by electroporation (Estacion et al., 2010). At 40 h after transfection, pyramidal neurons with robust GFP fluorescence were used for voltage-clamp recording. Pipette resistances were 1.1–2.6 MΩ. After break-in, neurons were held at −80 mV, and voltage-clamp recordings were conducted as described above.

*Data analysis.* Electrophysiology data were analyzed using Clampfit 9.2 (Molecular Devices), Excel (Microsoft), and OriginPro 8.1 (OriginLab), and are presented as mean values ± SEM. One-way ANOVA or Kruskal–Wallis nonparametric test, as indicated, was used for statistical analysis of $Na_v1.6_R$ WT, $Na_v1.6$-EGFP, and $Na_v1.6_R$-mCherry channels to compare EGFP intensities at the AISs of different $Na_v1.6$-EGFP mutants in neurons.

## Results

### The ankG-binding AIS targeting motif is sufficient to localize proteins to nodes of Ranvier *in vitro*

A 33 aa sequence within L2 of VGSCs is highly conserved among vertebrate homologs (Fig. 1). The proximal half of this sequence is rich in valine (V) and proline (P) residues and the distal half is rich in glutamic acid (E) and serine (S) residues, with a central invariant glutamic acid (E1111 in rat $Na_v1.2$ and E1100 in mouse

$Na_v1.6$) separating the proximal and distal parts of this motif. This conserved sequence has been reported to bind ankG and target reporter chimeric proteins to the AIS (Garrido et al., 2003; Lemaillet et al., 2003; Fache et al., 2004), a process that is regulated by CK2 phosphorylation of the conserved serine residues in this motif (Bréchet et al., 2008). The sequence is highly divergent in $Na_v1.9$ channels and is missing the N-terminal 5 aa residues in orthologs of the cardiac channel $Na_v1.5$.

Although the molecular compositions of the AIS and nodes of Ranvier are very similar, the mechanisms regulating their formation are different. AIS assembly is controlled by intrinsic mechanisms in neurons, whereas node formation requires interactions between myelinating glial cells and neurons (Salzer, 2003; Hedstrom and Rasband, 2006; Ogawa and Rasband, 2008). To test whether the ankG-binding AIS targeting motif is sufficient to localize proteins not only to the AIS but also to nodes of Ranvier, we used an *in vitro* rat DRG neuron–Schwann cell myelinating coculture system. We transfected cultured DRG neurons with constructs for chimeric proteins CD4-EGFP, CD4-$Na_v1.2$/L2-EGFP [CD4-L2-EGFP (Garrido et al., 2003)] or CD4-L2(ΔABD)-EGFP with 9 aa residues VPIALGESD essential for interacting with ankG removed from L2 (Lemaillet et al., 2003), and then induced myelination. Nodes and heminodes were identified by their ankG immunostaining (Fig. 2*A–C*). We found that CD4-EGFP and CD4-L2(ΔABD)-EGFP were distributed along the axons and not enriched at nodes or heminodes [$n = 63$ for CD4-EGFP; $n = 122$ for CD4-L2(ΔABD)-EGFP] (Fig. 2*A*,*B*,*D*). In contrast, although low levels of CD4-L2-EGFP were evident throughout the axons, we found that it was enriched at 61.3% (111 of 181) of ankG-positive nodes (Fig. 2*C*,*D*), indicating that the ankG-binding AIS targeting motif is sufficient for localization of the chimera to nodes of Ranvier.

However, CD4-L2-EGFP was not enriched in 38.7% (70 of 181) of the ankG-positive nodes. This likely results from the heterogeneity of myelination and node formation in the *in vitro* myelinating coculture system and is consistent with the idea that ankG clusters at nodes earlier than VGSCs and in turn recruits VGSCs (Jenkins and Bennett, 2002). Together with the limitations of studies using channel fragments, these results emphasize the need to use full-length VGSCs *in vivo* to assess the essentiality of the ankG-binding motif for AIS and nodal clustering of sodium channels.

### Fluorescently tagged $Na_v1.6$ channels are targeted to the AIS in cultured hippocampal neurons

A fluorescent probe for investigating targeting of $Na_v1.6$ in native neurons was generated by fusing EGFP or mCherry fluorescent proteins to the C terminus of full-length mouse $Na_v1.6$ (channel rendered TTX-R as described in Materials and Methods). Functional analysis in the DRG-derived neuronal cell line ND7/23 using whole-cell voltage clamp in the presence of 300 nM TTX to block endogenous voltage-gated sodium currents (Fig. 3*A*,*B*; Table 1) shows that the fusion of either EGFP or mCherry to the C terminus of $Na_v1.6$ does not change channel biogenesis or gating properties.

Expression of the $Na_v1.6$-EGFP and $Na_v1.6$-mCherry channels in hippocampal neurons resulted in a robust fluorescence after 6 d in culture. $Na_v1.6$-EGFP (Fig. 3*C*) and $Na_v1.6$-mCherry (Fig. 3*D*) were enriched at the AIS delineated by ankG immunostaining, whereas only weak fluorescence was detectable in the somatodendritic compartment, which was marked by MAP2 immunostaining. Thus, the EGFP- or mCherry-fused $Na_v1.6$ channels could be used to evaluate the role of the ankG-binding motif in channel targeting to axonal compartments.

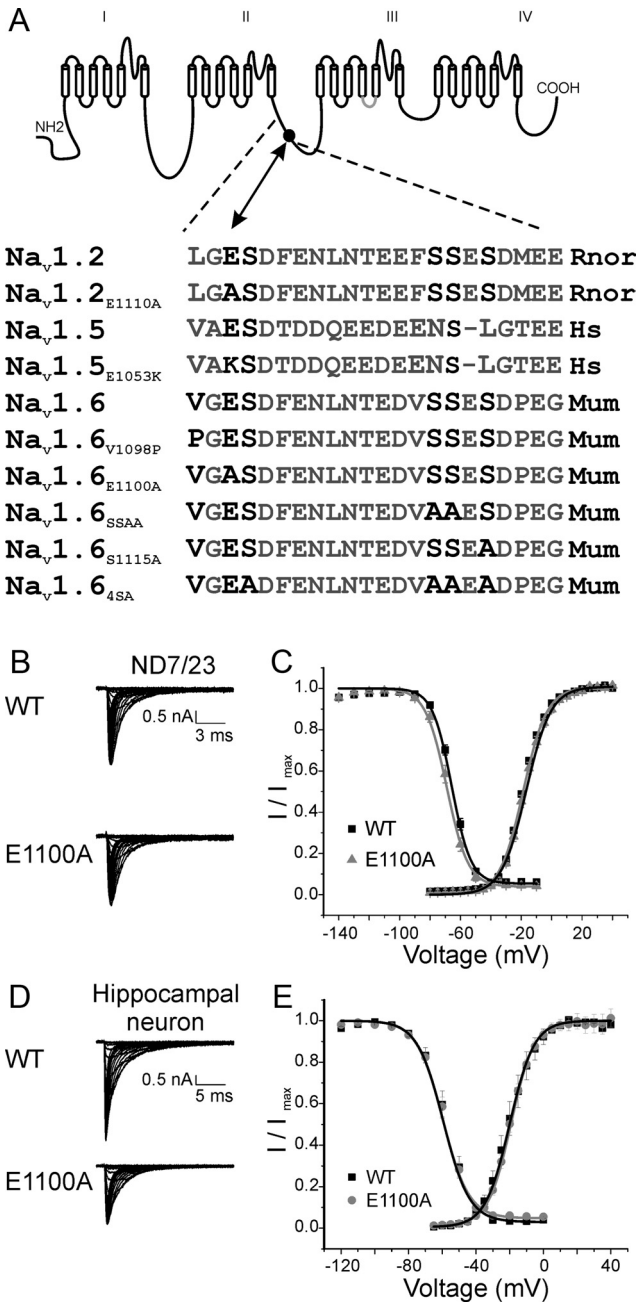


**Figure 4.** $Na_v1.6$-EA-EGFP mutant channels have gating properties similar to those of wild-type $Na_v1.6$-EGFP channels. ***A***, Schematic of the $\alpha$-subunit of sodium channel showing the 24 transmembrane segments and loops with the ankG-binding motif in loop 2 (L2) delineated by broken line, and the invariant glutamic acid residue (E1110 in $Na_v1.2$, E1053 in $Na_v1.5$, and E1100 in $Na_v1.6$) designated by the solid circle. The other $Na_v1.6$ mutant channels used in this study are shown for completeness. ***B***, Representative sodium currents of individual ND7/23 cells expressing $Na_v1.6$-EGFP and$Na_v1.6$-EA-EGFP channels. No significant difference in current density between WT and mutant channels was observed. ***C***, The voltage dependence of activation and steady-state fast-inactivation of $Na_v1.6$-EGFP (black square), and $Na_v1.6$-EA-EGFP (gray triangle) channels; steady-state inactivation was measured following a 500 ms prepulse. Activation and steady-state fast-inactivation of mutant channels were similar to those of WT channels. ***D***, Representative sodium currents of individual transfected P0–P5 rat hippocampal neurons expressing $Na_v1.6$-EGFP or $Na_v1.6$-EA-EGFP channels. Current density of the mutant channel was approximately one-half that of WT channels. ***E***, Voltage dependence of activation and steady-state fast-inactivation of $Na_v1.6$-EGFP (black square) and $Na_v1.6$-EA-EGFP (gray circle); steady-state fast-inactivation was measured following a 100 ms prepulse. Activation and steady-state fast-inactivation of mutant channels were similar to those of WT channels. Numerical values are presented in Table 1.

**Table 2. Expression of WT and $Na_v1.6$-EA-EGFP channels in rat hippocampal neurons**

| | | | Activation | | | Steady-state fast-inactivation | | | |
|---|---|---|---|---|---|---|---|---|---|
| | Current density at −5 mV (pA/pF) | Reversal potential (mV) | $V_{1/2,act}$ | $k$ | $n$ | $V_{1/2,fast}$ | $k$ | $A(\%)^a$ | $n$ |
| WT | 465 ± 70 (17) | 70.6 ± 1.7 | −20.2 ± 2.6 | −6.85 ± 0.27 | 8 | −57.7 ± 2.0 | 6.65 ± 0.30 | 2.64 ± 0.62 | 10 |
| E1100A | 238 ± 33 (16)* | 68.3 ± 1.4 | −20.0 ± 1.1 | −6.79 ± 0.29 | 10 | −58.4 ± 1.4 | 7.16 ± 0.24 | 4.57 ± 1.20 | 10 |

[a]Percentage of channels that do not enter into a fast-inactivated state.

*$p < 0.05$, $Na_v1.6$-EA-EGFP versus WT channels.

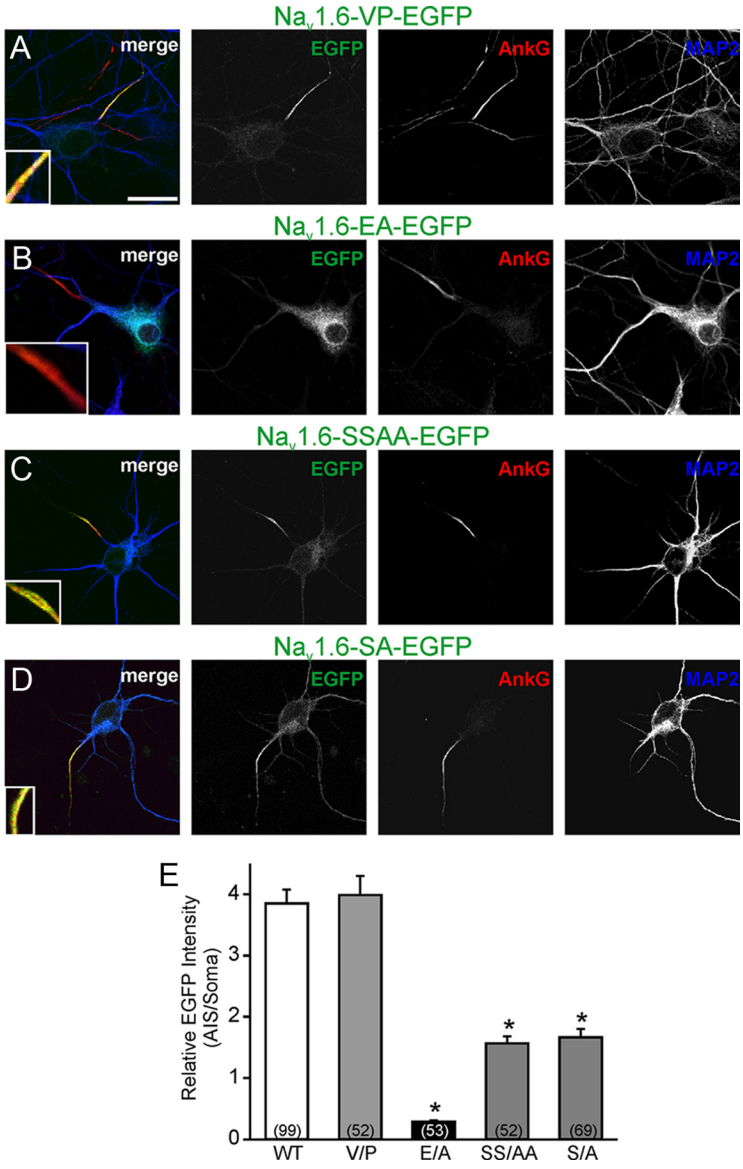


**Figure 5.** E1100 within the ankG-binding motif in $Na_v1.6$/L2 is necessary for channel targeting to the AIS in cultured hippocampal neurons. ***A–D***, Localization of fluorescently tagged $Na_v1.6$-EGFP carrying mutations within the ankG-binding motif in rat hippocampal neurons. V1098P (VP) did not impair targeting of $Na_v1.6$ to the AIS (***A***); the inset is a 4× magnification of the AIS region that highlights colocalization of $Na_v1.6$-VP-EGFP and ankG (yellow). E1100A (EA) completely disrupted localization of $Na_v1.6$ at the AIS (***B***); the inset is a 4× magnification of the AIS region that highlights the fact that $Na_v1.6$-EA-EGFP is excluded from the ankG-positive AIS (red). Mutations of the CK2 sites S1112A and S1113A (SSAA; ***C***) or S1115A (SA; ***D***) partially impaired targeting of $Na_v1.6$ to the AIS; the insets are a 4× magnification of the AIS region that highlight colocalization of $Na_v1.6$-SSAA-EGFP and $Na_v1.6$-SA-EGFP with ankG (yellow). Scale bar, 20 $\mu$m. ***E***, To measure $Na_v1.6$ localization at the AISs, relative EGFP intensities were quantified with ImageJ software. Two regions of interest representing either the AISs (ankG immunostaining) or a somatodendritic region (MAP2 immunostaining) were defined, and the average EGFP intensity of the AIS region was then normalized to the average EGFP intensity of the somatodendritic region. Total numbers of analyzed cells are indicated in parentheses. Data are shown as mean values ± SEM, and the asterisk (*) indicates $p < 0.05$ by Kruskal–Wallis nonparametric test compared with localization of the EGFP-tagged wild-type channel.

### Mutations in the ankG-binding motif produce functional channels

Previous studies have implicated the invariant glutamic acid residue in the central segment of the AIS targeting motif (E1100 in $Na_v1.6$; amino acid coordinates hereafter are for mouse $Na_v1.6$ sequence) and nearby CK2 phosphorylation sites (S1101, S1112–S1113, and S1115) in regulating the targeting of $K_v2.1$ chimera reporter proteins to the AIS (Fache et al., 2004; Bréchet et al., 2008), and the mutation of the equivalent glutamic acid residue in the cardiac sodium channel $Na_v1.5$-E1053K (Fig. 4*A*) has been identified in a patient with Brugada syndrome (Mohler et al., 2004). Sequence analysis of mammalian VGSCs shows that a proline residue is present at the equivalent position of valine 1098 within the proximal AIS targeting motif of $Na_v1.7$ (Fig. 1). Based on its biophysical properties, $Na_v1.7$ is thought to be a threshold channel that is better suited to nerve terminals where it boosts subthreshold stimuli, rather than at the AIS or nodes of Ranvier (Rush et al., 2007). Thus, we reasoned that V1098 might also regulate AIS targeting. To validate the role of these residues in targeting full-length sodium channels, we introduced the substitutions V1098P (VP), E1100A (EA), S1112–1113A (SSAA), S1115A (SA), and S1101A/S1112–1113A/S1115A (4SA) into $Na_v1.6$-EGFP channels (Fig. 4*A*) and investigated the localization of the mutant channels at the AISs and nodes of Ranvier.

To verify that the introduced mutations did not impair channel function, the currents of the mutant versions of $Na_v1.6$-EGFP were analyzed by voltage-clamp following transient transfection of the neuronal cell line ND7/23. Data in Figure 4, *B* and *C*, and Table 1 show that none of the mutations significantly changed peak current amplitudes or voltage-dependence of activation or steady-state fast-inactivation, indicating that the mutant channels retained wild-type properties.

The $Na_v1.5$-E1053K ankG-binding defective mutant channel produced sodium currents when expressed in HEK293 cells, but failed to be inserted in the plasma membrane of cardiac myocytes (Mohler et al., 2004). Thus, we evaluated the insertion of functional

$Na_v1.6$-EA-EGFP mutant channels in the plasma membrane of transfected hippocampal neurons using whole-cell voltage-clamp recording. The $Na_v1.6$-EA-EGFP mutant channels produced currents with comparable properties of activation and fast inactivation to those of WT channels (Fig. 4*D*,*E*), but only one-half of the current density (Table 2). Thus, while the E1100A mutation reduces the steady-state levels of $Na_v1.6$ channels at the plasma membrane, it does not completely trap the channel in cytoplasmic compartments.

### Targeting of $Na_v1.6$ *in vitro* depends on E1100 within the ankG-binding motif

Hippocampal neurons were transfected with wild-type and mutants channels, and AIS localization was assessed by costaining with MAP2 and ankG (Fig. 5). The proficiency of channel targeting to the AIS was assessed by calculating the ratio of the signal intensity at the AIS to that within the somatodendritic compartments, as described in Materials and Methods. The V1098P substitution did not alter AIS localization [Fig. 5*A*,*E*; 3.98 ± 0.31 arbitrary units (AU); $n = 52$] compared with the wild-type channel (Figs. 3*C*, 5*E*; 3.86 ± 0.21 AU; $n = 99$). In contrast, the E1100A substitution caused the mutant channel to accumulate in the somatodendritic compartment and completely abrogated enrichment of $Na_v1.6$-EGFP at the AIS (Fig. 5*B*,*E*; 0.29 ± 0.02 AU; $n = 53$; $p < 0.05$). Channels carrying mutations of the CK2 phosphorylation sites, $Na_v1.6$-SSAA-EGFP (Fig. 5*C*,*E*; 1.55 ± 0.13 AU; $n = 52$) or $Na_v1.6$-SA-EGFP (Fig. 5*D*,*E*; 1.66 ± 0.14 AU; $n = 69$), had significantly impaired enrichment of the channel at the AIS ($p < 0.05$), but, in contrast to the E1100A substitution, these mutations did not completely block AIS targeting.

To exclude any possible artifact related to the overexpression of tagged, mutant $Na_v1.6$ channels in individual neurons, we coexpressed mutant $Na_v1.6$-EGFP and wild-type $Na_v1.6$-mCherry in the same cell. As expected, wild-type $Na_v1.6$-EGFP and $Na_v1.6$-mCherry channels colocalized at the AIS in transfected neurons (Fig. 6*A*). Similarly, the $Na_v1.6$-VP-EGFP mutant channels colocalized with the wild-type $Na_v1.6$-mCherry channels (Fig. 6*B*). In contrast, $Na_v1.6$-EA-EGFP mutant channels were mainly detected in the somatodendritic compartment (Fig. 6*C*, green), whereas the wild-type $Na_v1.6$-mCherry showed the expected AIS accumulation and colocalized with ankG (Fig. 6*C*, magenta). The mutant channels $Na_v1.6$-SSAA-EGFP or $Na_v1.6$-SA-EGFP did not perturb AIS localization of $Na_v1.6$-mCherry, although the enrichment of the mutant channels at the AIS versus the somatodendritic compartment was reduced (Fig. 6*D*,*E*).

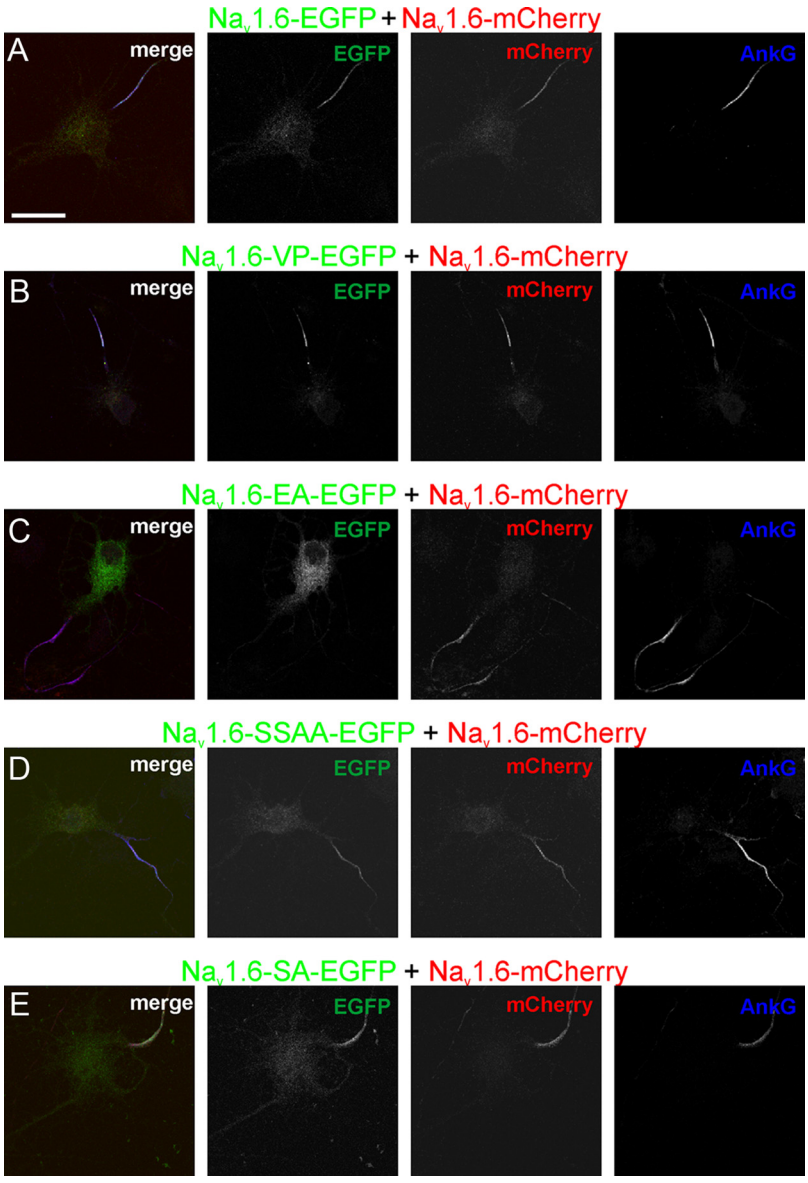


**Figure 6.** AIS targeting of wild-type $Na_v1.6$-mCherry and mutant derivatives of $Na_v1.6$-EGFP following simultaneous transfection of hippocampal neurons. ***A–E***, Rat hippocampal neurons were simultaneously transfected with WT or $Na_v1.6$ carrying different mutations fused to EGFP (green), and wild-type $Na_v1.6$ fused to mCherry (red). After 6 d in culture, AISs in transfected cells were stained for ankG (blue), and localization of the fluorescently tagged channels was analyzed by confocal microscopy. ***A***, Hippocampal neurons simultaneously transfected with WT $Na_v1.6$-EGFP and $Na_v1.6$-mCherry constructs showed colocalization of green and red fluorescence at the AIS. ***B***, $Na_v1.6$-VP-EGFP, colocalized with $Na_v1.6$-mCherry at the AISs labeled by ankG. ***C***, $Na_v1.6$-EA-EGFP mutant channels show uniform distribution within the somatodendritic neuronal compartment and no enrichment at the AIS, whereas wild-type $Na_v1.6$-mCherry was localized at the AIS in the same cell. ***D***, ***E***, $Na_v1.6$-SSAA-EGFP (***D***) and $Na_v1.6$-SA-EGFP (***E***) channels carrying mutant CK2 phosphorylation sites are coclustered with $Na_v1.6$-mCherry at the AIS. Scale bar, 20 $\mu$m.

### Mutation of E1100 blocks clustering of $Na_v1.6$ channels at axon initial segments *in vivo*

To validate these results *in vivo*, we used *in utero* coelectroporation in E14 mouse brains to express $Na_v1.6$-EGFP or $Na_v1.6$-EGFP mutants together with wild-type $Na_v1.6$-mCherry channels. After electroporated mice were born, we collected and analyzed their brains for transfected neurons at P5 (Fig. 7*A–D*) and at P27 (Fig. 7*E*). We found a very high degree of coelectroporation (86%; 238 of 278) in transfected neurons within the somatosensory cortex, with both $Na_v1.6$-EGFP and $Na_v1.6$-mCherry immunoreactivity present at the AIS of transfected cells (Fig. 7*A*, arrowheads). Our data show that the

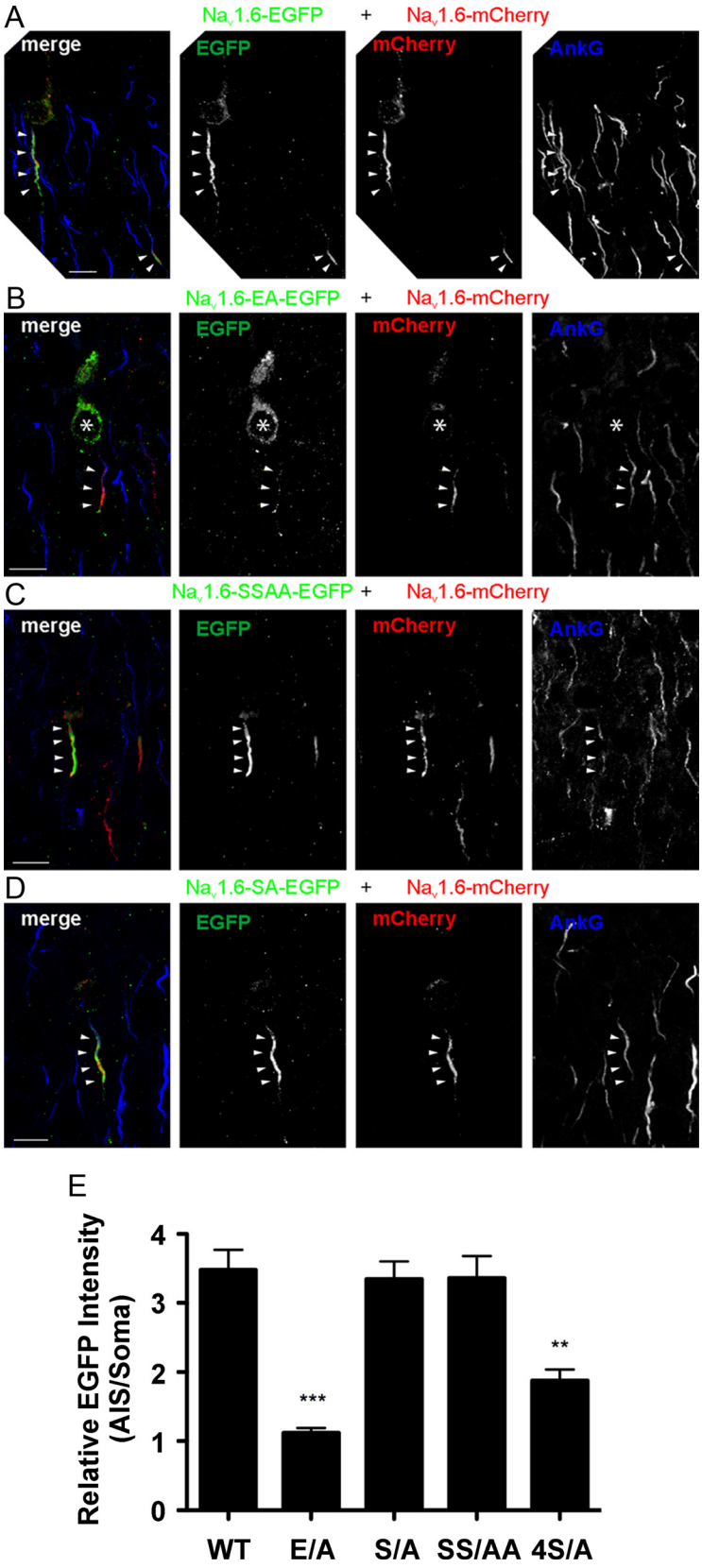


**Figure 7.** E1100A but not S1112–1113A or S1115A regulate targeting of $Na_v1.6$ to the AIS *in vivo*. ***A–D***, Plasmids encoding full-length $Na_v1.6$ channels fused to mCherry ($Na_v1.6$-mCherry) were coelectroporated *in utero* at E14 into mouse embryonic brains together with wild-type $Na_v1.6$-EGFP (***A***), $Na_v1.6$-EA-EGFP (***B***), $Na_v1.6$-SSAA-EGFP (***C***), or $Na_v1.6$-SA-EGFP (***D***). Neurons within the somatosensory cortex were analyzed at postnatal day 5. AnkG immunostaining (blue) was used to label the AIS, and the arrowheads indicate the AIS of cotransfected neurons. ***E***, Quantification of the ratio of AIS to somatic EGFP immunoreactivity in neurons within the somatosensory cortex were analyzed at postnatal day 27 for wild-type (WT) ($n = 11$), $Na_v1.6$-EA-EGFP ($n = 12$), $Na_v1.6$-SSAA-EGFP ($n = 14$), $Na_v1.6$-SA-EGFP ($n = 14$), or $Na_v1.6$–4SA-EGFP ($n = 10$) channels. The AIS was delineated by the $Na_v1.6$-mCherry signal. Scale bar, 20 $\mu$m. Data are shown as mean values ± SEM. ***$p < 0.0001$ and **$p < 0.001$ by ANOVA compared with localization of the EGFP-tagged wild-type channel.

$Na_v1.6$-EA-EGFP mutant channel was not enriched at the AIS (Fig. 7*B*, arrowheads); instead EGFP immunoreactivity was located throughout the cell soma and in the primary apical dendrite (Fig. 7*B*, asterisk). However, in partial agreement with our *in vitro* results, we found that the CK2 mutant channels $Na_v1.6$-SSAA-EGFP and $Na_v1.6$-SA-EGFP were efficiently clustered at the AIS (Fig. 7*C*,*D*, arrowheads). Figure 7*E* shows that the measured AIS/soma EGFP fluorescence intensity ratio for $Na_v1.6$-SSAA-EGFP (3.36 ± 0.32 AU; $n = 14$) and $Na_v1.6$-SA-EGFP (3.35 ± 0.26 AU; $n = 14$) are not significantly different from that of wild-type $Na_v1.6$-EGFP (3.48 ± 0.29 AU; $n = 11$). However, the intensity ratio for the $Na_v1.6$-EA-EGFP mutant channel (1.12 ± 0.07 AU; $n = 12$) was significantly ($p < 0.0001$) different from that of the wild-type channel.

In a separate experiment, we tested the hypothesis that simultaneous mutation of the four CK2 residues within the ankG-binding motif may be necessary to unmask a CK2 phosphorylation effect on channel targeting *in vivo*. The $Na_v1.6$–4SA-EGFP channels are localized to the AIS in transfected hippocampal neurons in culture (Fig. 8*A–D*) and *in vivo* (Fig. 8*E*), indicating that they are not essential for channel localization to the AIS. However, quantification of the $Na_v1.6$–4SA-EGFP signal at the AIS *in vivo* appears to be impaired compared with $Na_v1.6$-EGFP channels (Fig. 7*E*; 1.88 ± 0.16 AU; $n = 10$; $p < 0.001$). Thus, in contrast to the case of $K_v2.1$-$Na_v1.2$/L2 (Bréchet et al., 2008), E1100A alone in the ankG-binding AIS targeting motif abrogates $Na_v1.6$ channel clustering at the AIS, whereas the quadruple serine mutations, but not single or double mutations impair channel clustering. Whether the single mutation S1101A underlies the effect observed for the 4SA mutation *in vivo* has not been formally ruled out.

### The ankG-binding motif is necessary for targeting of $Na_v1.6$ channels to nodes of Ranvier *in vivo*

AIS and nodes of Ranvier share many ion channels, cell adhesion molecules, and cy-

toskeletal scaffolds (Ogawa and Rasband, 2008). However, one major difference between these two sites is that AIS are intrinsically specified by neurons, while VGSC clustering at nodes requires extrinsic factors from myelinating glia. We asked whether the clustering of $Na_v1.6$ channels at nodes requires the ankG-binding AIS targeting motif *in vivo*, by examining mouse brains electroporated *in utero* with $Na_v1.6$-EGFP mutants and wild-type $Na_v1.6$-mCherry, and then analyzed at P27, a time point chosen to allow for myelination and formation of mature nodes of Ranvier. In this experiment, we identified nodes of Ranvier by Caspr immunoreactivity at paranodes and the coelectroporated wild-type $Na_v1.6$-mCherry at nodes. As for AIS localization, we found that the $Na_v1.6$-EA-EGFP mutant channel did not cluster at nodes of Ranvier (Fig. 9*A*, blue, arrowhead), but the $Na_v1.6$-mCherry was efficiently clustered at nodes (Fig. 9*A*, green, arrowhead). We also found that the $Na_v1.6$-SSAA-EGFP and $Na_v1.6$-SA-EGFP mutant channels were efficiently clustered at nodes of Ranvier (Fig. 9*B*,*C*, respectively, arrowheads). Unlike $Na_v1.6$-EA-EGFP channels (Fig. 9*A*), $Na_v1.6-4SA$-EGFP channels were detected at nodes of Ranvier (Fig. 8*E*). These observations demonstrate that the ankG-binding AIS targeting motif in $Na_v1.6$ channels is necessary for their clustering at nodes of Ranvier *in vivo*, but that CK2 phosphorylation is not essential.

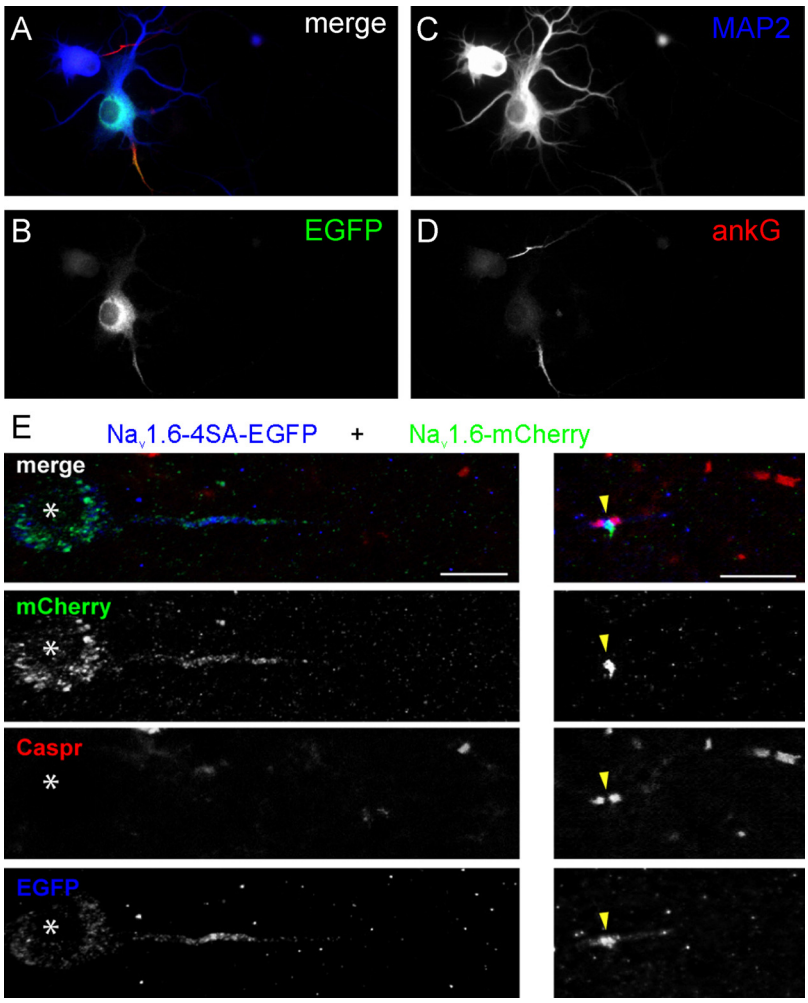


**Figure 8.** The four CK2 phosphorylation sites within the ankG-binding motif are not essential for targeting of $Na_v1.6$ to the AIS or nodes of Ranvier. ***A–D***, Rat hippocampal neurons were transfected with fluorescently tagged $Na_v1.6-4SA$-EGFP mutant channels carrying the quadruple mutation of the four CK2 sites [S1101A, SS1112–1113AA, and S1115A (4SA)] within the ankG-binding motif. The $Na_v1.6-4SA$-EGFP mutant channels (***B***) colocalize with ankG (***D***) at the AIS (***A***, merge). The somatodendritic compartment is labeled with MAP2 (***C***). Mutations of the four CK2 sites did not block accumulation of the mutant channel at the AIS. ***E***, Plasmids encoding full-length $Na_v1.6$ channels fused to mCherry ($Na_v1.6$-mCherry) were coelectroporated *in utero* at E14 into mouse embryonic brains together with $Na_v1.6-4SA$-EGFP mutant channels. Neurons within the somatosensory cortex were analyzed at postnatal day 27. Caspr immunostaining (red) was used to label paranodes, and arrowheads indicate a node of Ranvier in cotransfected neurons. The asterisks indicate the cell body of the cotransfected neuron. WT $Na_v1.6$-mCherry is shown in green, and $Na_v1.6$-4SA-EGFP mutant is shown in blue. Scale bar, 10 $\mu$m.

## Discussion

The precise clustering of VGSCs at the AIS and nodes of Ranvier in myelinated axons is crucial for efficient action potential initiation and propagation, respectively. In the present study, we evaluated molecular determinants for AIS and nodal targeting in the ankG-binding motif in L2 of VGSCs using full-length $Na_v1.6$ channels. Fluorescently tagged functional channels were properly localized at the AIS and nodes of Ranvier in cultured neurons and *in vivo* following *in utero* electroporation of mouse brains. Importantly, the single E1100A substitution within the central segment of the ankG-binding motif in L2 was sufficient to prevent accumulation of $Na_v1.6$ at the AIS and nodes of Ranvier. While single (S1112A) and double (S1112–1113A/S1115A) mutations of CK2 phosphorylation sites had only partial effects *in vitro*, and did not affect AIS or nodal clustering *in vivo*, the quadruple mutation [S1101A/S1112–1113A/S1115A (4SA)] reduced AIS localization *in vivo*. The wild-type and mutant channels used here generated currents with identical properties, indicating that the observed effects on channel localization did not result from gross changes in channel folding or modulation. Our study demonstrates the dominant role of a single critical residue within the ankG-binding motif for proper and efficient targeting of $Na_v1.6$ to the expected axonal compartments and the feasibility of studying trafficking, retention, and clustering of VGSCs in axonal compartments using full-length channels *in vivo*.

A critical role for the invariant glutamic acid residue within the ankG-binding motif (E1100 in $Na_v1.6$) in sodium channel targeting and ankG binding is supported by the characterization of a naturally occurring and disease-producing mutation of the equivalent residue in the cardiac sodium channel $Na_v1.5$ (E1053K; Fig. 4*A*) in Brugada syndrome (Mohler et al., 2004). In partial agreement with data showing that $Na_v1.5$-E1053K channels are not transported to the surface of the cardiac myocytes (Mohler et al., 2004), the current density of $Na_v1.6$-E1100A channels in hippocampal neurons was ~50% that of wild-type channels. Additionally, $Na_v1.5$-E1053K showed altered gating properties compared with wild-type channels when expressed in HEK293 cells (Mohler et al., 2004), while our data (Tables 1, 2) showed similar gating properties for wild-type and $Na_v1.6$-E1100A channels in hippocampal neurons and ND7/23 neuronal cell line. It is not unreasonable to suggest that the

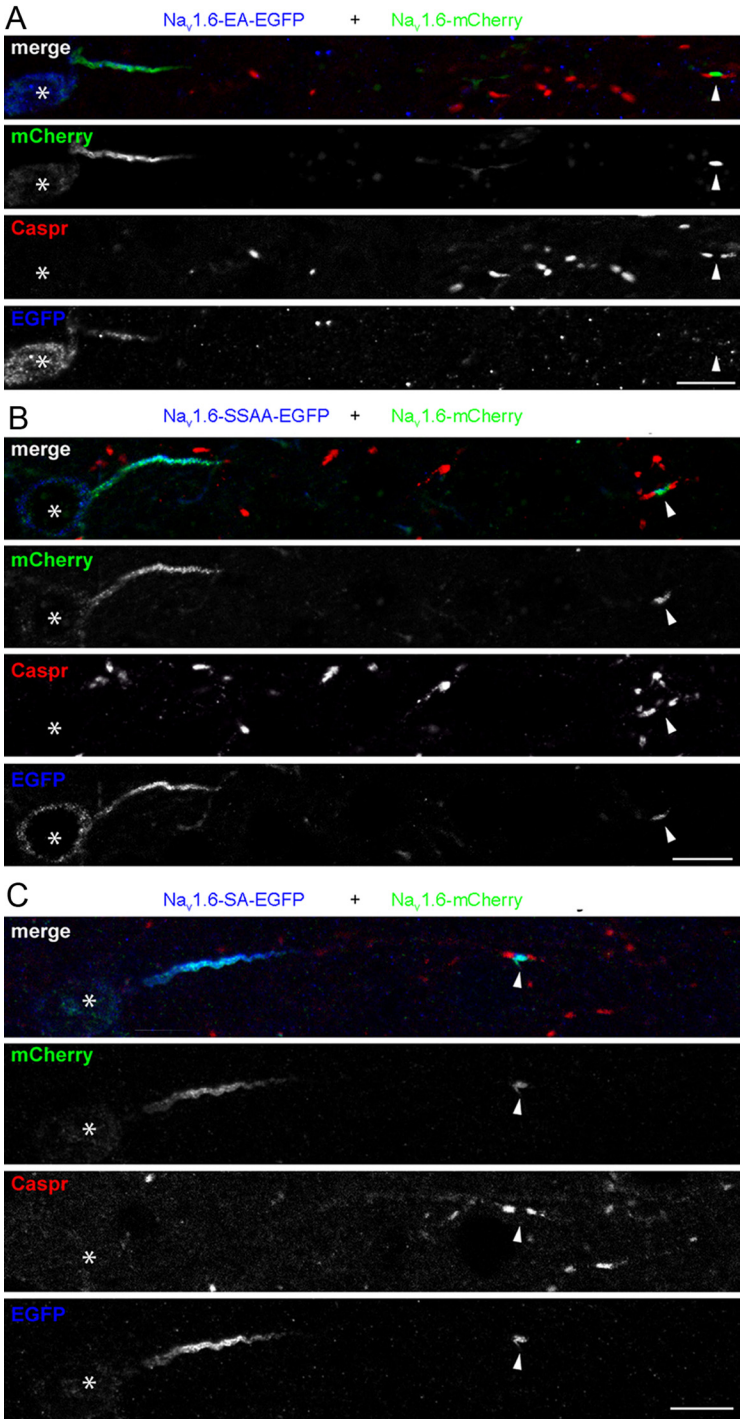


**Figure 9.** AIS targeting motif and interaction with ankG are necessary for $Na_v1.6$ clustering at nodes of Ranvier *in vivo*. ***A–C***, Plasmids encoding full-length wild-type Nav1.6 channels fused to mCherry ($Na_v1.6$-mCherry) were coelectroporated *in utero* at E14 into mouse embryonic brains together with $Na_v1.6$-EA-EGFP (***A***), $Na_v1.6$-SSAA-EGFP (***B***), or $Na_v1.6$-SA-EGFP (***C***). Caspr immunostaining (red) was used to label paranodes, and the arrowheads indicate a node of Ranvier corresponding to cotransfected neurons. The asterisks indicate the cell body of the cotransfected neuron. Brains were analyzed at postnatal day 27. WT $Na_v1.6$-mCherry is shown in green, and $Na_v1.6$-EGFP mutants are shown in blue. Scale bar, 10 $\mu$m.

difference might be caused by the size or chemical properties of the side groups of the substituted residue in the mutant channel: lysine ($Na_v1.5$-E1053K) compared with alanine ($Na_v1.6$-E1100A). Together, these data support a dominant role for the invariant glutamic acid residue within the central segment of the ankG-binding motif in accumulation of VGSCs at ankG-dependent neuronal and muscle localization sites.

The VGSC composition of the AIS varies among different neuronal cell types, with $Na_v1.2$ and $Na_v1.6$ being predominant in most CNS neurons (Vacher et al., 2008). Previous work studying VGSC localization in the somatodendritic domain and the AIS used chimeric reporter proteins, which consisted of NF-186, CD4, or $K_v2.1$ fused to fragments of $Na_v1.2$ or $Na_v1.6$ (Garrido et al., 2003; Lemaillet et al., 2003; Fache et al., 2004; Bréchet et al., 2008). These studies showed that the L2 segments of VGSCs carry an ankG-binding motif that is sufficient for localization of these reporter proteins within the AIS. We now show that the ankG-binding motif is also sufficient to target a CD4-L2-EGFP chimeric protein to nodes of Ranvier in a myelinating DRG neuron–Schwann cell coculture. Interestingly, the presence of CD4-L2-EGFP in the internodes underlying the myelin sheaths (Fig. 2) suggests that domains other than L2 are required to restrict VGSCs to nodes.

Our data showing that E1100 is essential for AIS and nodal targeting of full-length $Na_v1.6$ are consistent with *in vivo* studies in ankG knock-out mice (Zhou et al., 1998; Jenkins and Bennett, 2001), and with shRNA knockdown studies in cultured hippocampal neurons, which have demonstrated that ankG is necessary for the initial recruitment and maintenance of sodium channels at the AIS (Hedstrom et al., 2007, 2008). Additionally, the essentiality of the E1100 for AIS and nodal targeting of full-length VGSCs shown in our study suggest that other interactions of the $\alpha$-subunits may not be sufficient to compensate for the loss of the interaction with AnkG. For example, the expected interaction of the $\alpha$- and $\beta$-subunits of sodium channels *in vivo* is not sufficient to substitute for the loss of ankG binding with the E1100A mutant channel for AIS and nodal targeting, even though $\beta$-subunits are known to interact with nodal proteins (Ratcliffe et al., 2001; Malhotra et al., 2002; McEwen and Isom, 2004). Together with the sufficiency of L2 in AIS and nodal targeting, our data show that the interaction of VGSCs with ankG is pivotal in their targeting to the axonal compartments.

However, chimeric proteins with a single transmembrane domain like NF-186 or CD4 can provide important information about the role of targeting motifs. AIS targeting of CD4/$Na_v1.2$ chimera was abolished by the single E1111A or E1111Q substitutions in the ankG-binding site (Fache et al., 2004), suggesting an important role for this residue in ankG binding. Recently, $K_v$ channel chimeras have been suggested as more appropriate to investigate ion channel targeting because they consist of multiple membrane-spanning

segments similar to the architecture of VGSCs and can be functionally assessed by recording potassium currents (Bréchet et al., 2008). In contrast to the CD4 chimeric data, AIS targeting of $K_v2.1/Na_v1.2$ reporters was only partially perturbed by the E1111A mutation (~90% of the AISs had the chimeric protein, including 40% showing somatodendritic accumulation in addition to AIS clustering), but was abolished by additional single and double mutations of CK2 phosphorylation sites within this motif (Bréchet et al., 2008). These findings highlight two major concerns for the use of $K_v2.1$ chimeric proteins in studying molecular determinants of VGSC targeting to the AIS and nodes. First, since $K_v2.1$ also accumulates at the AIS of hippocampal neurons in culture (Sarmiere et al., 2008), the use of $K_v2.1/Na_v1.2$-L2 chimeras makes it difficult to distinguish between intrinsic $K_v2.1$ channel AIS clustering and clustering that can be attributed to the localization motif of VGSCs. Second, $K_v2.1/Na_v1.2$-L2 chimeric channels are composed of four identical subunits and therefore have four AIS localization motifs for each assembled channel. CK2-mediated phosphorylation of residues within this motif may strengthen the interaction of E1111A mutant chimeric proteins with ankG, thus requiring the combination of E1110A and CK2 mutations to abrogate AIS clustering of the chimeric protein (Bréchet et al., 2008). Native VGSCs are composed of four nonidentical domains and carry a single ankG-binding motif within L2, more like the CD4 and NF186 chimeras where the mutation of the E1100 alone is sufficient to impair channel clustering at the AISs, a finding that is in agreement with our results presented here. Our data, however, support the possibility that CK2-dependent phosphorylation also contributes to channel clustering and, in particular, might increase the affinity of the VGSCs for ankG (Bréchet et al., 2008), because the $Na_v1.6$–4SA-EGFP mutant channels, but not channels with the single or double serine substitutions, manifested impaired clustering at the AIS.

Our study shows that nodal and AIS targeting of $Na_v1.6$ depends on an intact binding site for ankG and that the invariant glutamic acid residue E1100 within this motif is essential for channel targeting *in vivo*. We have also demonstrated the feasibility of studying targeting of full-length ion channels in neurons both in culture and *in vivo*. This is especially important because the folded structure of specific intracellular regions of VGSCs may not be recapitulated within reporter proteins due to constraints by flanking transmembrane segments and possible intramolecular interactions of different channel segments. Together, our results show that an intact ankG-binding motif is both necessary and sufficient for clustering of $Na_v1.6$ to both the AIS and nodes of Ranvier.

## References


Bennett V, Lambert S (1999) Physiological roles of axonal ankyrins in survival of premyelinated axons and localization of voltage-gated sodium channels. J Neurocytol 28:303–318.

Black JA, Renganathan M, Waxman SG (2002) Sodium channel $Na_v1.6$ is expressed along nonmyelinated axons and it contributes to conduction. Mol Brain Res 105:19–28.

Boiko T, Rasband MN, Levinson SR, Caldwell JH, Mandel G, Trimmer JS, Matthews G (2001) Compact myelin dictates the differential targeting of two sodium channel isoforms in the same axon. Neuron 30:91–104.

Bréchet A, Fache MP, Brachet A, Ferracci G, Baude A, Irondelle M, Pereira S, Leterrier C, Dargent B (2008) Protein kinase CK2 contributes to the organization of sodium channels in axonal membranes by regulating their interactions with ankyrin G. J Cell Biol 183:1101–1114.

Burgess DL, Kohrman DC, Galt J, Plummer NW, Jones JM, Spear B, Meisler MH (1995) Mutation of a new sodium channel gene, Scn8a, in the mouse mutant "motor endplate disease." Nat Genet 10:461–465.

Dzhashiashvili Y, Zhang Y, Galinska J, Lam I, Grumet M, Salzer JL (2007) Nodes of Ranvier and axon initial segments are ankyrin G-dependent domains that assemble by distinct mechanisms. J Cell Biol 177:857–870.

Estacion M, Gasser A, Dib-Hajj SD, Waxman SG (2010) A sodium channel mutation linked to epilepsy increases ramp and persistent current of Nav1.3 and induces hyperexcitability in hippocampal neurons. Exp Neurol 224:362–368.

Fache MP, Moussif A, Fernandes F, Giraud P, Garrido JJ, Dargent B (2004) Endocytotic elimination and domain-selective tethering constitute a potential mechanism of protein segregation at the axonal initial segment. J Cell Biol 166:571–578.

Fried SI, Lasker AC, Desai NJ, Eddington DK, Rizzo JF 3rd (2009) Axonal sodium channel bands shape the response to electric stimulation in retinal ganglion cells. J Neurophysiol 101:1972–1987.

Garrido JJ, Giraud P, Carlier E, Fernandes F, Moussif A, Fache MP, Debanne D, Dargent B (2003) A targeting motif involved in sodium channel clustering at the axonal initial segment. Science 300:2091–2094.

Grubb MS, Burrone J (2010) Activity-dependent relocation of the axon initial segment fine-tunes neuronal excitability. Nature 465:1070–1074.

Hedstrom KL, Rasband MN (2006) Intrinsic and extrinsic determinants of ion channel localization in neurons. J Neurochem 98:1345–1352.

Hedstrom KL, Xu X, Ogawa Y, Frischknecht R, Seidenbecher CI, Shrager P, Rasband MN (2007) Neurofascin assembles a specialized extracellular matrix at the axon initial segment. J Cell Biol 178:875–886.

Hedstrom KL, Ogawa Y, Rasband MN (2008) AnkyrinG is required for maintenance of the axon initial segment and neuronal polarity. J Cell Biol 183:635–640.

Herzog RI, Cummins TR, Ghassemi F, Dib-Hajj SD, Waxman SG (2003) Distinct repriming and closed-state inactivation kinetics of Nav1.6 and Nav1.7 sodium channels in mouse spinal sensory neurons. J Physiol 551:741–750.

Hille B (2001) Ion channels of excitable membranes, Ed 3. Sunderland, MA: Sinauer Associates.

Jenkins SM, Bennett V (2001) Ankyrin-G coordinates assembly of the spectrin-based membrane skeleton, voltage-gated sodium channels, and L1 CAMs at Purkinje neuron initial segments. J Cell Biol 155:739–746.

Jenkins SM, Bennett V (2002) Developing nodes of Ranvier are defined by ankyrin-G clustering and are independent of paranodal axoglial adhesion. Proc Natl Acad Sci U S A 99:2303–2308.

Kaplan MR, Cho MH, Ullian EM, Isom LL, Levinson SR, Barres BA (2001) Differential control of clustering of the sodium channels $Na_v1.2$ and $Na_v1.6$ at developing CNS nodes of Ranvier. Neuron 30:105–119.

Kuba H, Oichi Y, Ohmori H (2010) Presynaptic activity regulates $Na^+$ channel distribution at the axon initial segment. Nature 465:1075–1078.

Lemaillet G, Walker B, Lambert S (2003) Identification of a conserved ankyrin-binding motif in the family of sodium channel alpha subunits. J Biol Chem 278:27333–27339.

Malhotra JD, Koopmann MC, Kazen-Gillespie KA, Fettman N, Hortsch M, Isom LL (2002) Structural requirements for interaction of sodium channel beta 1 subunits with ankyrin. J Biol Chem 277:26681–26688.

McEwen DP, Isom LL (2004) Heterophilic interactions of sodium channel beta 1 subunits with axonal and glial cell adhesion molecules. J Biol Chem 279:52744–52752.

Mohler PJ, Rivolta I, Napolitano C, LeMaillet G, Lambert S, Priori SG, Bennett V (2004) $Na_v1.5$ E1053K mutation causing Brugada syndrome blocks binding to ankyrin-G and expression of $Na_v1.5$ on the surface of cardiomyocytes. Proc Natl Acad Sci U S A 101:17533–17538.

Ogawa Y, Rasband MN (2008) The functional organization and assembly of the axon initial segment. Curr Opin Neurobiol 18:307–313.

Ratcliffe CF, Westenbroek RE, Curtis R, Catterall WA (2001) Sodium channel beta1 and beta3 subunits associate with neurofascin through their extracellular immunoglobulin-like domain. J Cell Biol 154:427–434.

Rush AM, Wittmack EK, Tyrrell L, Black JA, Dib-Hajj SD, Waxman SG (2006) Differential modulation of sodium channel $Na_v1.6$ by two members of the fibroblast growth factor homologous factor 2 subfamily. Eur J Neurosci 23:2551–2562.

Rush AM, Cummins TR, Waxman SG (2007) Multiple sodium channels and their roles in electrogenesis within dorsal root ganglion neurons. J Physiol 579:1–14.

Salzer JL (2003) Polarized domains of myelinated axons. Neuron 40:297–318.

Sarmiere PD, Weigle CM, Tamkun MM (2008) The Kv2.1 $K^+$ channel targets to the axon initial segment of hippocampal and cortical neurons in culture and in situ. BMC Neurosci 9:112.

Schafer DP, Custer AW, Shrager P, Rasband MN (2006) Early events in node of Ranvier formation during myelination and remyelination in the PNS. Neuron Glia Biol 2:69–79.

Susuki K, Raphael AR, Ogawa Y, Stankewich MC, Peles E, Talbot WS, Rasband MN (2011) Schwann cell spectrins modulate peripheral nerve myelination. Proc Natl Acad Sci U S A 108:8009–8014.

Vacher H, Mohapatra DP, Trimmer JS (2008) Localization and targeting of voltage-dependent ion channels in mammalian central neurons. Physiol Rev 88:1407–1447.

Wittmack EK, Rush AM, Craner MJ, Goldfarb M, Waxman SG, Dib-Hajj SD (2004) Fibroblast growth factor homologous factor 2B: association with Nav1.6 and selective colocalization at nodes of Ranvier of dorsal root axons. J Neurosci 24:6765–6775.

Wittmack EK, Rush AM, Hudmon A, Waxman SG, Dib-Hajj SD (2005) Voltage-gated sodium channel Nav1.6 is modulated by p38 mitogen-activated protein kinase. J Neurosci 25:6621–6630.

Zhou D, Lambert S, Malen PL, Carpenter S, Boland LM, Bennett V (1998) AnkyrinG is required for clustering of voltage-gated Na channels at axon initial segments and for normal action potential firing. J Cell Biol 143:1295–1304.